Battery-Free Wireless Video Streaming Camera System

Ali Saffari[1], Mehrdad Hessar[2], Saman Naderiparizi[1] and Joshua R. Smith[1,2]
[1]Electrical and Computer Engineering Department and [2]Paul G. Allen School of Computer Science and Engineering
University of Washington, Seattle, USA-98195
{saffaria, mehrdadh, samannp, jrsjrs}@uw.edu

***Abstract*—We design and prototype the first battery-free video streaming camera that harvests energy from both ambient light and RF signals. The RF signals are emitted by a nearby access point. The camera collects energy from both sources and backscatters up to 13 frames per second (fps) video at a distance of up to 150 ft in both outdoor and indoor environments. Compared to a single harvester powered by either ambient light or RF, our dual harvester design improves the camera's frame rate. Also, the dual harvester design maintains a steady 3 fps at distances beyond the RF energy harvesting range. To show efficacy of our battery-free video streaming camera for real applications such as surveillance and monitoring, we deploy our camera for a day-long experiment, from 8 AM to 4 PM, in an outdoor environment. Our results show that on a sunny day, our camera can provide a frame rate of up to 9 fps using a 4.5 cm×2.2 cm solar cell.**

I. Introduction

Battery-free wireless sensors have been actively researched for many years. Advancements in this area have led to the development of battery-free low throughput/low-power sensors for temperature, light and pressure [7], [27] as well as high throughput/more power hungry sensors such as cameras. Over the past few years, researchers have shown that we can harvest sufficient power from ambient energy sources such as Wi-Fi and RFID readers to power off-the-shelf low resolution cameras. While harvested power can capture still images, it is insufficient for video streaming [19].

The critical obstacle preventing systems such as the WISP-Cam [19] from streaming live video is the camera's high power consumption. Conventional camera architectures consist of an array of photo-diodes that sense the image, a high bandwidth and low-noise amplifier (LNA) that amplifies the signal generated by the photo-diodes, and a high rate analog-to-digital converter (ADC) that digitizes the amplifier output. For many digital video streaming applications, a video compression module is also necessary to reduce required communication bandwidth. Note that most camera power consumption results from the use of power hungry components including the LNA, ADC and compression module [14], [20].

More recently, researchers have redesigned the conventional camera architecture to remove power hungry components from the camera and delegate them to a wireless access point (AP) in an asymmetric wireless communication setting such as backscatter [16]. In [16], the raw analog voltage generated by the pixels is converted into a pulse width modulated (PWM) signal and then fed into the backscatter module, avoiding the power hungry components of a camera such as the ADC and amplifier. Although this design is very low power, the prototype built in [16] does not operate based on harvested energy. Therefore, building an end-to-end system that can harvest its energy from ambient sources and stream video to a wireless AP remained an unsolved challenge.

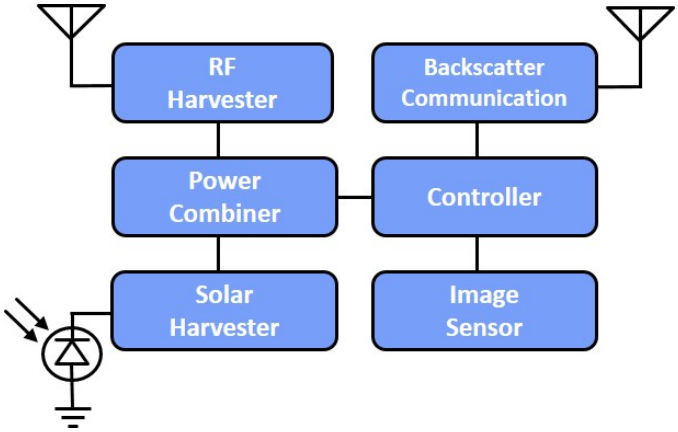

Fig. 1: **Battery-Free, Wireless Video Streaming Architecture.** We design a battery-free video streaming camera that harvests both RF and solar power.

Further, although the redesigned camera architecture reduces the power a conventional camera consumes by a few orders of magnitude, existing off-the-shelf cameras [5] that best match the proposed architecture still burn more power than is harvestable from an FCC-compliant RF source at useful ranges. In reality, we can harvest micro-watt level power from an FCC-compliant RF source at medium to far distances (a few feet to a few tens of feet); however, aforementioned cameras burn a few mW. Bridging the gap between available harvested power and required power would enable the design of security and monitoring cameras that do not require wires, thereby significantly reducing infrastructure installation and maintenance costs. A battery-free video streaming camera can also provide a monitoring system for hard-to-reach areas and energy-constrained applications, such as Kilobots and insect-scale robots [11], [26].

This paper presents the first battery-free camera that streams

978-1-7281-1210-7/19/$31.00 ©2019 IEEE

978-1-7281-1210-7/19/$31.00 ©2019 IEEE

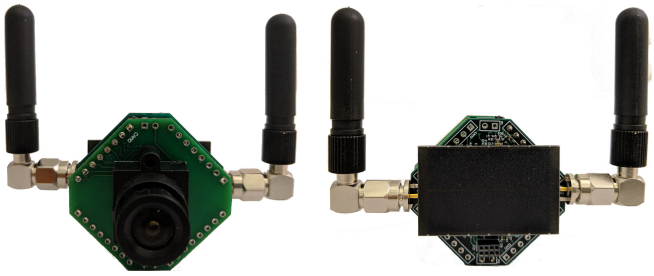

Fig. 2: **Prototype for Our Battery-Free Video Streaming Camera with Dual Power Harvester.** The FPGA is located behind the solar cell.

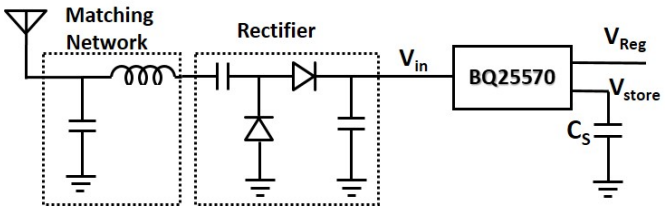

Fig. 3: **RF Harvesting Circuit.**

live video to a wireless AP and harvests all of its energy by aggregating ambient light and RF. Fig. 1 shows our system architecture. We evaluated the video streaming camera in indoor and outdoor environments under different lighting conditions. In outdoor scenarios on a sunny day, our camera can stream 13 fps live video to the AP using a 2.2 cm$\times$0.7 cm solar cell. In indoor scenarios under normal office lighting conditions (about 500 lux), our camera can stream at > 5 fps live video at a distance of up to 10 ft, leveraging both RF and ambient light energy harvesting, and 3 fps at a distance of up to 150 ft, mainly relying on light energy harvesting.

To show the feasibility of our video streaming camera for real applications (e.g., a surveillance or monitoring camera), we build a battery-free camera that streams video to a nearby AP. We set up our camera outside a building on a sunny day and record video frames backscattered by the camera for eight hours. We show that our camera can backscatter video frames at 1 to 9 fps during a day when light intensity remains between 300 and 3000 lux. We implement a prototype of our battery-free video streaming camera using a 112$\times$112 image sensor controlled by an IGLOO nano FPGA, as shown in Fig. 2.

Our Contributions. Here, we list our main contributions:

- We develop the world's first battery-free and wire-free live video streaming system.
- We design and evaluate a dual energy harvester that aggregates energy from both ambient light and RF signals.
- We demonstrate a dual antenna architecture one used for energy harvesting and the other for communication that increases wireless communication and RF power harvesting range compared to a single antenna counterpart.

II. Related Work

Related work falls into two categories, backscatter communication and power harvesting, which we now describe.

Backscatter communication. Previous research in backscatter [10], [12], [13], [23] shows high data rate backscatter communication using Wi-Fi, Bluetooth or TV broadcast signals. Some research [34] designs a high data rate QAM backscatter modulator that works in the UHF band. Other work [35], [36] focuses on optimizing data flow operation from a sensor to a backscatter communication module to reduce power consumption. These works use an ADC to convert a sensor's analog output to digital information that is transmitted using digital backscatter. As noted in section I, for high throughput sensors such as cameras, ADCs are the primary power-consuming component of the system.

More recent research [9], [30] is demonstrating that backscatter is a feasible vehicle for wide-area, low-power communication. This work focuses on low data rate communication optimized for Internet-of-Things applications, which can scale to hundreds of devices in wide-area scenarios. However, it provides a throughput that is far too low for an application like video streaming.

In this work, we leverage a technique called analog backscatter [31], [33]. This technique transmits raw analog signals generated by a sensor, here an image sensor, and hence does not require key power consumers like an ADC. Furthermore, analog backscatter is viable for high-throughput applications such as video streaming. We build on previous works [8], [16] to design a battery-free video streaming camera that removes the power-hungry components from the sensor node and delegates them to a plugged-in access point.

Power harvesting. In the RF power harvesting domain, some research [15], [25] harvests energy from ambient TV signals. Other work [32] presents a power harvesting system that uses RF signals from Wi-Fi transmissions or prototypes a wireless sensing platform that harvests energy from TV broadcast signals and cellular base transceiver stations [24]. In [31], researchers design a battery-free cellphone that harvests energy from either RF or ambient light, but it does not combine both. Previous work on low-power camera design [18], [19], [21] builds battery-free wireless cameras that capture still images and backscatter the pixels to a nearby RFID reader. These works, based on the WISP [29] platform, send a frame every ten seconds when the camera is about one foot from the RF source and every tens of minutes at longer distances.

Finally, [22] demonstrates a large form-factor, low-resolution camera that harvests energy from incident light and captures one frame per second. The image is sent via cable to a computer. In contrast, our work shows a fully wireless, battery-free video streaming camera that harvests energy by combining power from both an RF signal and ambient light.

III. System Design and Implementation

Our battery-free camera contains five key components, as shown in Fig. 1: 1) an RF and a solar power harvester, 2) power combiner, 3) controller, 4) image sensor, and 5) backscatter communication system. The camera harvests energy from both the RF signal and ambient light and combines the energy. The AP generates a single-tone RF signal, which the camera uses

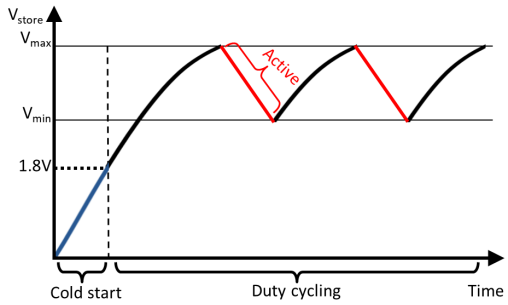

Fig. 4: **Power Harvesting Duty Cycle.** The power harvester IC stores energy on the capacitor. Once the voltage reaches V_{max}, the harvester powers the camera until the capacitor discharges to V_{min}.

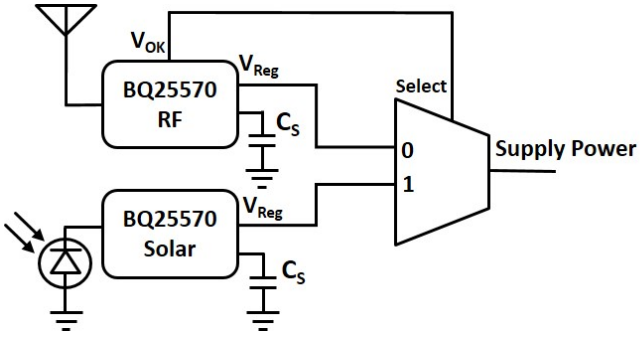

Fig. 5: **Dual Power Harvesting Architecture.** A dual power harvesting circuit that stores RF and solar power for our battery-free video streaming camera.

for RF energy harvesting and backscattering the video frames. This section explains each design component.

RF power harvester. As Fig. 3 shows the RF harvester includes three key components: 1) a matching network, 2) rectifier, and 3) and power harvester. The matching network matches antenna impedance to the conjugate of rectifier impedance. We use a single-stage high frequency LC network with the values of $L = 33\ nH$ and $C = 5.1\ pF$. After this matching, the RF signal goes to a full-wave rectifier, which converts the RF signal to DC voltage [32]. We use 33 pF capacitors and HSMS-285C [2] diodes to implement the rectifier.

Finally, the rectifier's output connects to a TI BQ25570 [4] energy harvester. To provide energy for the camera, this buck/boost charger IC operates in a forced duty-cycling mode that corresponds to the input power. As shown in Fig. 4, the harvester accumulates energy on a storage capacitor. When the voltage of the capacitor, V_{store} in Fig. 3, reaches a programmable threshold (V_{max}), the buck converter activates and supplies power from the storage capacitor to the camera until the capacitor discharges to another programmable threshold (V_{min}). Thus, the amount of stored energy during one cycle can be calculated from equation (1)

$$E = \frac{1}{2} C_S \left(V_{max}^2 - V_{min}^2 \right) \tag{1}$$

Considering the minimum voltage for camera operation and the voltage drop on the buck converter, we set $V_{min} \geq 3.4V$. Capacitor leakage current increases as its voltage increases; therefore, to preserve harvested power, we set $V_{min} = 3.4V$. We now have two knobs that can change the amount of energy supplied to our battery-free video streaming camera in each duty cycle, V_{max} and C_S.

The harvester begins from a cold start until V_{store} reaches $1.8\ V$, after which, the maximum power point tracking (MPPT) inside the BQ begins to operate. The MPPT enhances RF power harvesting efficiency by optimizing BQ input impedance. During the cold start, the minimum rectified voltage from which the BQ can still harvest energy is $330\ mV$. When V_{store} crosses $1.8\ V$, the MPPT activates and reduces the minimum required rectified voltage to $100\ mV$.

Dual RF-Solar power harvester. As shown in Fig. 8, relying only on RF energy harvesting from an FCC-compliant RF source forces the battery-free video streaming camera to be located within 17 ft of the AP. In addition, the camera cannot produce frames at a rate that exceeds 1 fps for distances beyond 9 ft, which limits the camera's utility and potential applications. As a result, RF power energy harvesting alone cannot unleash the potential that battery-free video streaming can provide.

To solve this problem, we combine RF with solar energy harvesting. For the latter, we use the same boost charger IC but without a rectifier since solar cell output is already a DC voltage. In an outdoor environment, our dual power harvester mainly relying on an unexposed-to-direct-sunlight solar cell with dimensions of 3.5 cm×4.2 cm can provide enough power for continuous video streaming at 13 fps. In an indoor environment, a dual power harvester provides sufficient power to achieve a frame rate that exceeds 5 fps at a distance of up to 10 ft from the access point using both the RF power harvester and a solar cell (9 cm×7.9 cm). This harvester also maintains a steady frame rate (3 fps) at farther distances, leveraging solar power harvesting in an indoor environment.

The key challenge to dual power harvesting is coordinating operation of two boost charger ICs in order to store energy from two different sources. As shown in Fig. 5, both ICs connect to the camera using an ADG774 analog multiplexer [1]. The harvesters work independently. Whenever any harvester stores enough energy, multiplexer selects that harvester to power the camera, giving the higher priority to the RF harvester. Thus, if both harvesters concurrently have enough energy, the camera first gets powered by RF harvested energy; and once this energy is consumed, the power source switches to harvested solar energy.

The BQ25570 IC activates a signal, named V_{OK}, when the harvester accumulates enough energy on the storage capacitor (C_S). We use V_{OK} here for the address input of the multiplexer. We use a fast multiplexer alongside a small capacitor at the input of the camera power supply to ensure negligible drops in camera supply voltage when switching between two harvesters. This guarantees that the camera does not brown out when switching occurs.

Image sensor. We use a 112×112 resolution gray-scale random pixel access image sensor from CentEye [5], which provides raw analog readout access to all the pixels. The image sensor has two internal "row" and "column" registers, which let the user output the raw analog voltage of a specific pixel. The analog voltage of this image sensor is a function of light intensity. We use this image sensor functionality to design our analog backscatter communication.

Controller. We use IGLOO nano, AGLN250V2 FPGA [3] to implement our controller state machine. To capture video frames, the FPGA sweeps through the pixels by setting the "row" and "column" registers' value in a raster-scan (row-by-row and left to right) mode. To generate the master clock for our battery-free camera state machine, we use an SiT802 [6] oscillator. This oscillator consumes only 180 μW of power in active mode, however, there is a 70 ms latency between oscillator power-up and when it outputs a clock signal. During this start-up period, FPGA operation is paused, and the image sensor remains in shut-down mode to save power. To design this part of our control system, we analyze two approaches and pick the one that lessens energy loss during oscillator start-up. We show the architectures for both approaches in Fig. 6.

First approach. Our goal here is to decrease the oscillator's start-up delay by never turning it off, instead forcing the oscillator to enter a standby mode when no operation is required. The SiT802 oscillator's standby mode consumes 4 μW of power and becomes active 3 ms after exiting from standby. In this approach, we supply power continuously to the oscillator but keep it in standby mode until the storage capacitor has reached V_{max} voltage. When the harvester accumulates enough energy on the storage capacitor to power up the camera, it outputs an enable signal (V_{OK}), which we use to enable the oscillator. As noted, switching between active and standby mode takes 3 ms, and, once the oscillator starts working, the FPGA initializes the image sensor. To do this, we must power: a voltage regulator to supply a regulated voltage to the oscillator, an inverter gate to invert the polarity of (V_{OK}) used to control the oscillator's operation mode, and the oscillator in standby mode. The regulator, inverter and oscillator in standby mode consume 2.5 μW, 3.5 μW, and 4 μW, respectively. The total energy consumed by these components when our system does not transmit any video frames is shown in equation (2)

$$E_1 = (P_{regulator}+P_{inverter}+P_{osc})\times t_{stb} = 10\times t_{stb}\ \mu J \quad (2)$$

where t_{stb} is the standby time.

Second approach. Here, to conserve energy during oscillator power up, we power the image sensor after the oscillator's 70 ms delay. To do this, we use a switch that is controlled by the FPGA and gates the power to the image sensor. We use an ADG774 [1] as the switch which consumes 3.3 μW. During the 70 ms delay, the FPGA is paused because the clock signal is not available; during this period, the FPGA consumes 240 μW. The oscillator's power is 180 μW in active mode. Equation (3) shows the energy consumption of this approach, where P_{FPGA} is the FPGA's power consumption when it is powered up with no clock source, and t_{delay} is the oscillator's delay.

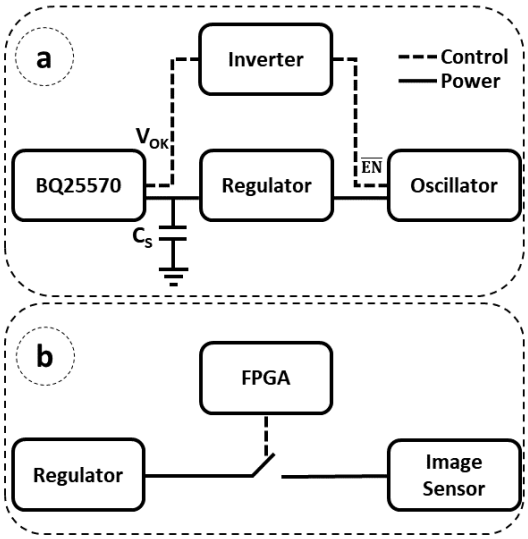

Fig. 6: **Proposed Architectures.** Alternative approaches for saving energy during oscillator start up.

$$E_2 = (P_{switch}+P_{FPGA}+P_{oscillator})\times t_{delay} \approx 29.6\ \mu J \quad (3)$$

Equating E_1 and E_2 provides the boundary condition that suggests which approach is more efficient in terms of energy loss. As a result, $t_{stb} = 2.96s$ (equivalently, frame rates > 0.34 fps) is the threshold below which *first approach* has a lower energy loss.

Backscatter communication. To transmit video frames to the access point, we use backscatter communication. A naive solution would connect image sensor output directly to an analog RF switch and use analog backscatter [33] to send video frames. However, the problem here is that the low dynamic range of the pixel voltages maps to a very small subset of radar cross-sections at the antenna. Assuming that both channel and receiver add noise to the signal, we would receive a low Signal to Noise Ratio (SNR) at the AP, which means that the communication range between the camera and the AP would be limited to short distances. Solving this dynamic range problem could be done using an Automatic Gain Control (AGC). However, this typically involves a power-hungry linear amplifier. Another approach could use a high-resolution ADC to convert the image sensor's analog voltage to a digital signal and send the video frames digitally, leveraging digital backscatter [19]. However, this alternative faces the same issues as the AGC approach and cannot meet our power constrains.

We choose to solve this problem using Pulse Width Modulation (PWM) to send video frames to the AP. This is equivalent to a single-bit ADC using PWM, whereby our analog data translates to the timing information of the pulses. In other words, the duty cycle of the pulses is defined by the analog voltage of raw pixel values. We design our PWM module using a passive RC block and a comparator.

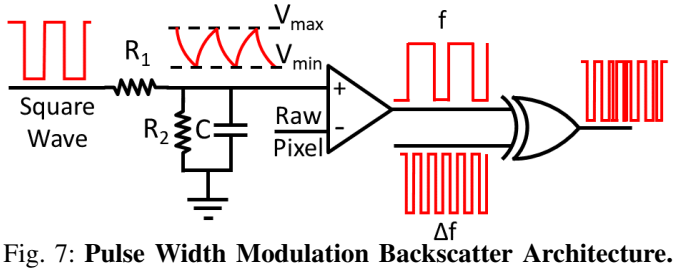

Fig. 7: **Pulse Width Modulation Backscatter Architecture.**

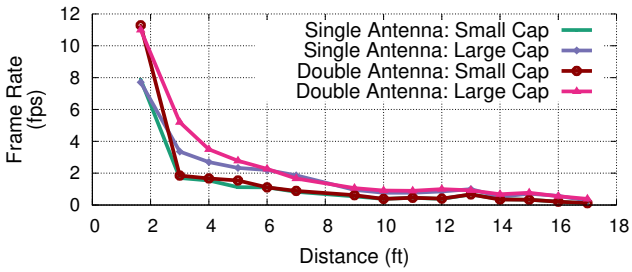

Fig. 8: **RF Harvesting Evaluation.** Frame rates of our video streaming camera at different distances when it is powered only by the RF harvester. Note that we define the frame rate as average number of frames over a short period of time (a few minutes).

Fig. 7 shows our PWM design. One way to generate a PWM encoded signal uses a triangular wave with a primary frequency of f as the reference and compares it to the raw information-containing signal [17]. Comparator output is a PWM signal with a primary frequency of f and a time-varying duty cycle proportional to the amplitude of the raw input signal.

Here, we use the FPGA to generate a square wave with a primary frequency of f and amplitude of A, which is then low-pass filtered to generate an approximated triangular wave. We can adjust the triangular wave's V_{max} and V_{min} by tuning R_1, R_2, C and A according to equations (4) and (5). During charging period, the capacitor's voltage increases from an initial V_{min} with time constant $\tau = (R1||R2)C$ to the maximum voltage of $V_{max} < V_M = AR_2/(R_1 + R_2)$. During discharge, the capacitor's voltage decreases from the initial V_{max} with the same time constant, τ.

$$V_{charging}(t) = (V_M - V_{min})(1 - e^{\frac{-t}{\tau}}) + V_{min} \quad (4)$$

$$V_{discharging}(t) = V_{max}e^{\frac{-t}{\tau}} \quad (5)$$

$$V_{max} = V_M(1 - e^{\frac{-1}{2f\tau}}) + V_{min}e^{\frac{-1}{2f\tau}} \quad (6)$$

$$V_{min} = V_{max}e^{\frac{-1}{2f\tau}} \quad (7)$$

By setting $t = 1/2f$, the triangular wave's maximum and minimum voltage can be calculated using equations (6) and (7). V_{max} and V_{min} should be set to ensure the image sensor's analog output falls within the V_{max} and V_{min} range. Finally, the triangular wave is compared to the image sensor's analog output. The comparator's output is a PWM signal whose duty-cycle is proportional to the analog voltage of the raw pixel. Equation (8) shows the duty cycle corresponding to analog pixel value P.

$$PWM(P) = 0.5 + f * \tau * ln(\frac{V_M - P}{V_M - V_{min}} * \frac{V_{max}}{P}) \quad (8)$$

A conventional challenge in backscatter-based communication systems is in-band interference caused by the transmitted single-tone RF signal. The receiver picks up this very strong signal and, if it falls in the communication band, its phase noise can completely overwhelm the received signal. To solve this problem, sub-carrier modulation is used to shift the backscattered information frequency spectrum. In our system, we use an XOR gate to shift the backscattered data frequency spectrum by Δf. We input our PWM signal and a square wave with the primary frequency of Δf to an XOR gate and the output is an up-converted version of the PWM signal. This technique addresses the self-interference problem, which increases the signal-to-noise ratio (SNR) and thus the operating range of our backscatter communication.

Dual antenna architecture. Our system uses two antennas: one connected to the RF harvester to harvest RF energy, and the second connected to an RF switch to enable backscatter communication. Previous design [19] uses a single antenna for both energy harvesting and backscatter communication, and loading of the antenna switches between short and matched impedance when backscattering. In our dual antenna design, loading of the backscatter antenna switches between open and short impedance, which are farther apart on the Smith Chart [28]. This results in a higher Delta Radar Cross-Section, improving the SNR and thus communication range of our dual antenna approach relative to a single antenna implementation.

IV. Evaluation and Application

We now evaluate multiple aspects of our battery-free video streaming camera. First, we assess our RF and solar power harvesting circuits. Next, we characterize the performance of our battery-free video streaming camera using our dual harvester design. We then show the video quality of our video streaming camera. Finally, we evaluate our system in a real application deployment.

RF harvesting evaluation. We deploy our video streaming device in a lab environment. We use a USRP X300 software-defined radio connected to a power amplifier to generate a single-tone RF signal. We set the power amplifier output to 30 dBm and connect it to a 6 dBi patch antenna to comply with FCC regulations for the 900 MHz ISM band. We evaluate our RF harvester for both single and dual antenna approaches.

For the single antenna approach, we use a 2 dBi whip antenna for both energy harvesting and backscatter communication and tune the matching network to ensure the antenna is matched to a 50 Ω load. We also evaluate RF energy harvesting in a dual antenna approach, assigning one antenna for backscatter communication and the other for energy harvesting.

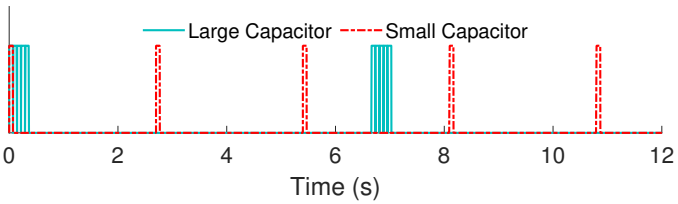

Fig. 9: **Time Domain Comparison of Video Frame Generation Using Different Capacitor Sizes.** A large capacitor produces bursts of frames, while a small one produces single frames at shorter intervals.

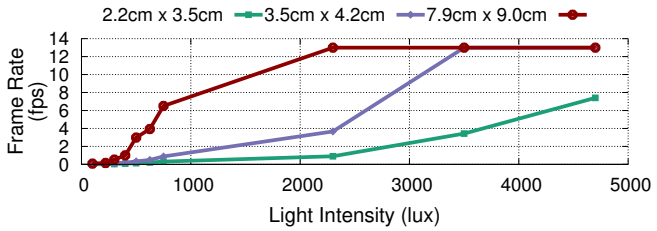

Fig. 10: **Solar Harvesting Evaluation.** The frame rate of our video streaming camera at different lighting conditions for three different solar cell sizes. We collect data for light intensity of $lux < 750$ in an office building and the rest in outdoor environment.

Fig. 8 shows the update rate of our battery-free video streaming camera at different distances from the AP. This plot shows that as distance increases, frame rate decreases. We also evaluate the RF harvester using a small or large storage capacitor. As shown in Fig. 8, using a large storage capacitor increases the frame rate in both cases. According to equation (1) increasing capacitor size results in storing more energy and therefore sending more video frames once the capacitor discharges. As a result, the controller must initialize the image sensor only once. In contrast, using a small capacitor results in repeated image sensor initialization for lower numbers of video frames. Thus, using a large capacitor increases the frame rate slightly; however, a large capacitor produces bursts of frames, while a small one produces single frames at shorter intervals. Fig. 9 shows the distribution of video frames over time.

We can achieve up to 12 fps at close distances when we use two antennas; in contrast, we achieve only 8 fps when we use the single antenna architecture. This is because during backscatter communication in the single antenna approach, the load connected to the antenna is modulated between a matched and short-circuit, causing reflection of some incident RF power rather than full absorption. In other words, during backscatter, RF to DC efficiency drops due to antenna load impedance modulation. However, at longer distances, the frame rates of the dual and single antenna approaches converge because the frame rate is very low and the battery-free camera spends a negligible period of time in backscatter mode.

Solar power harvesting. We next evaluate the performance of our video streaming camera powered by the solar power harvester. In this experiment, we use a small capacitor. We evaluate our system indoors and outdoors under different lighting conditions. Fig. 10 shows the results for three different solar cells with dimensions of $2.2\ cm \times 3.5\ cm$, $3.5\ cm \times 4.2\ cm$, and $7.9\ cm \times 9\ cm$. In indoor scenarios, under normal office lightning conditions ($lux \approx 500$), our camera transmits up to 3 fps video frames. However, in an outdoor environment with a light intensity of $lux > 4500$ (not exposed to direct sunlight), our video camera backscatters 8 fps video using the solar cell with the smallest surface area.

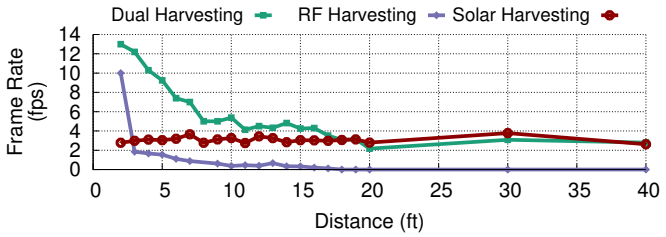

Fig. 11: **Dual Power Harvesting Evaluation.** Video streaming camera operating with a single or dual power harvesting source. Note that we show this plot up to 40 ft to better represent our results at near distances. This result will persist up to 150 ft with the same trend as we see after 20 ft.

Dual power harvesting. To evaluate our dual harvester video streaming camera, we use a USRP X300 software-defined radio connected to a power amplifier to generate a 30 dBm single-tone signal at 900 MHz into a 6 dBi antenna and to receive the backscattered video frames from the camera. We use two 2 dBi whip antennas for RF harvesting and backscatter communication. For the solar harvester, we use a halogen lamp to provide a light intensity of 500 lux at the surface of the solar cell. We connect a $9\ cm \times 7.9\ cm$ solar cell to our solar power harvester and use separate small capacitors for each power harvester to ensure the camera sends only one frame when the storage capacitor is charged to V_{max}.

To perform this evaluation, we vary the distance between the camera and the AP and measure the frame rate of our battery-free video streaming camera which is powered by the dual power harvester. Fig. 11 shows the frame rate of the camera at different distances; we also show the frame rate of the camera when it is powered by the solar harvester at fixed 500 lux and by the RF harvester. We learn the following from this plot:

- Up to a distance of 18 ft, where the RF power harvester stops working, we observe a monotonically decreasing frame rate as the distance increases. After the distance of 18 ft, the frame rate becomes almost constant because the camera is being powered only by the solar cell, which is independent of the distance to the AP. At very close distances (less than 8 ft), the camera harvests a considerable amount of energy from the RF source, bringing the frame rate up to about 13 fps at 2 ft.
- The frame rate of the dual harvester is greater than the sum of the frame rate of individual harvesters because individual harvesters must initialize the image sensor every time they power up the camera; thus, they use some

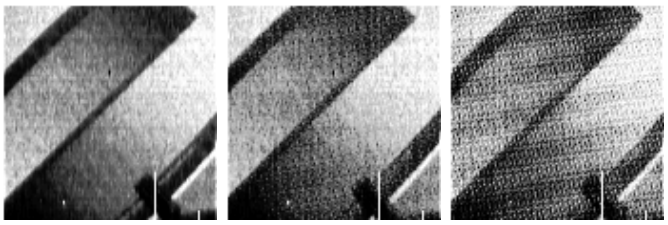

(a) Baseline (b) $PSNR = 33\ dB$ (c) $PSNR = 28\ dB$

Fig. 12: **Sample Video Frames.** Video frames from our video streaming camera at different PSNR values.

of the stored energy for initialization. In contrast, for the dual harvester, the time during which the RF harvester provides energy can overlap with the time during which the solar harvester powers up the camera. Therefore, the camera remains on and does not need to initialize the image sensor. Instead, it uses initialization energy to send more video frames to the AP.

Analog video quality. To evaluate the video quality of our backscatter communication system, we power our video streaming camera with a battery. We use a USRP connected to a power amplifier as the AP to transmit 30 dBm single-tone signal at 900 Mhz into a 6 dBi antenna and receive the backscattered video frames from the camera. We vary the distance between the camera and AP and, at each distance, we send a 20 s video clip at a rate of 13 fps. To collect the ground-truth video, we record the camera's output with a National Instrument USB-6361 DAQ. We use the PSNR metric to evaluate our received video quality using PWM backscatter communication. We calculate PSNR using received video frames at the AP and recorded data with the DAQ. As a rule of thumb, video frames with a PSNR of 25 dB or higher are considered to be acceptable frame quality compared to the ground-truth. We plot snapshots of video frames for a gray-scale ramp image in Fig. 12, which are recorded with our video streaming camera along with corresponding PSNR values to show the quality of our recorded video.

Fig. 13 shows PSNR at different distances in a room with low lighting conditions ($lux = 100 - 200$). In general, as distance increases, PSNR decreases as well. However, due to multipath effects, at some locations the PSNR increases as distance increases. The average PSNR of the received signal is greater than 22.5 dB at a distance of up to 150 feet from the AP. Beyond this distance, the USRP cannot decode the frames reliably since the SNR of backscatterd video from the camera falls below the minimum required SNR at the receiver input.

Application deployment. Wireless cameras are very popular for security applications and smart home monitoring systems. However, existing wireless cameras must either be plugged in or require frequent battery replacement/recharging. To demonstrate our battery-free video camera's applicability for surveillance and home monitoring applications, we deploy our dual-harvester battery-free camera in an outdoor environment, connect a solar cell with dimensions of 4.5 cm×2.2 cm to the solar harvester, and use a USRP X300 as the AP. We set up

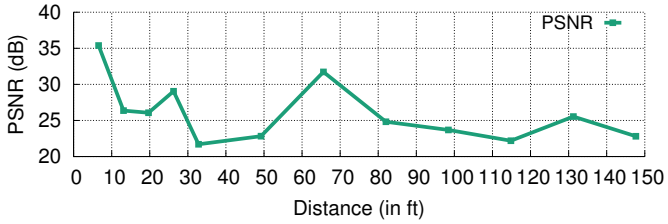

Fig. 13: **Analog Video Quality.** The quality of backscattered video frames over distance using the PSNR metric.

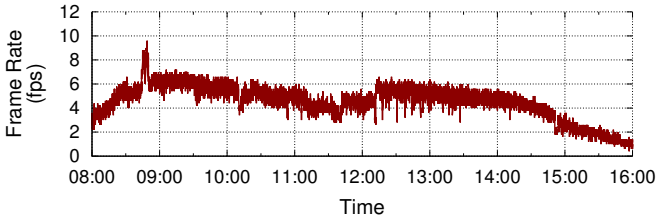

Fig. 14: **Application Deployment.** Video streaming frame rate achieved by our battery-free video camera over the course of eight hours.

our camera at the distance of 10 ft from the AP and record video frames from 8 AM to 4 PM during a sunny day where light intensity changes over time. Fig. 14 shows the frame rate of our battery-free video streaming camera during this eight hours of operation. The camera provides video at frame rates that vary between 1 fps and 9 fps depending on power availability. We expect that the solar harvester provides power that varies at a lower rate than the power provided by the RF harvester, because the AP is placed in a lab environment with people moving around. Thus, jitters observed in the frame rate are caused by abrupt changes in the RF power absorbed by the RF harvester.

Before 8 AM and after 4 PM, the amount of available solar energy is insufficient and the camera is powered only by the RF harvester. In this case, since the distance between the camera and the AP is 10 ft, our battery-free video streaming camera sends video frames to the AP with the frame rate of 0.4 fps.

V. Conclusion

This paper presented the first battery-free video streaming camera with a dual power harvester that combines energy from both light and RF sources. By combining RF and light power, we achieved a higher frame rate at short distances compared to an RF-only power harvester. In addition, the use of solar power harvesting increased the operating range of our battery-free video camera to the point where it was no longer limited by RF power harvesting. We proposed a video streaming architecture with two separate antennas for backscatter communication and RF power harvesting to increase the efficiency of our RF power harvester and improve the range of backscatter communication. Finally, we deployed our video streaming camera for a day-long experiment, showing its potential for surveillance and monitoring applications.

VI. Acknowledgements

We thank the anonymous reviewers for their helpful feedback on the paper. Also, we thank Ali Najafi, Vikram Iyer, and Mohamad Katanbaf for their comments on the paper. This work was funded in part by ARPA-E 1556660 (DE-AR0000938) and NSF CRI award CNS-1823148.

References

[1] Adg774 analog switch datasheet, 2004. https://www.analog.com/en/products/adg774.html.

[2] Hsms-285c schottky diode datasheet, 2009. https://www.broadcom.com/products/wireless/diodes/schottky/hsms-285c.

[3] Igloo nano agln250v2 fpga datasheet, 2015. https://www.microsemi.com/existing-parts/parts/142445.

[4] Ti bq25570 harvester datasheet, 2015. http://www.ti.com/product/BQ25570.

[5] Centeye stonyman image sensor datasheet, 2017. http://www.centeye.com/products/current-cen teye-vision-chips/.

[6] Sitime oscillator datasheet, 2017. https://www.sitime.com/products/1-26-mhz-oscillators/sit8021.

[7] Tire pressure and brake temperature systems smartstem, Accessed November 2018. http://www.craneae.com/Products/Sensing/SmartStem.aspx.

[8] M. Hessar, S. Naderiparizi, Y. Wang, A. Saffari, S. Gollakota, and J. R. Smith. Wireless video streaming for ultra-low-power cameras. In *Proceedings of the 16th Annual International Conference on Mobile Systems, Applications, and Services*, pages 536–536. ACM, 2018.

[9] M. Hessar, A. Najafi, and S. Gollakota. Netscatter: Enabling large-scale backscatter networks. In *16th USENIX Symposium on Networked Systems Design and Implementation (NSDI 19)*, 2019.

[10] V. Iyer, V. Talla, B. Kellogg, S. Gollakota, and J. Smith. Inter-technology backscatter: Towards internet connectivity for implanted devices. In *Proceedings of the 2016 ACM SIGCOMM Conference*.

[11] J. James, V. Iyer, Y. Chukewad, S. Gollakota, and S. B. Fuller. Liftoff of a 190 mg laser-powered aerial vehicle: The lightest wireless robot to fly.

[12] B. Kellogg, A. Parks, S. Gollakota, J. R. Smith, and D. Wetherall. Wi-fi backscatter: Internet connectivity for rf-powered devices. In *Proceedings of the 2014 ACM Conference on SIGCOMM*.

[13] B. Kellogg, V. Talla, S. Gollakota, and J. R. Smith. Passive wi-fi: Bringing low power to wi-fi transmissions. In *NSDI 16*.

[14] R. LiKamWa, B. Priyantha, M. Philipose, L. Zhong, and P. Bahl. Energy characterization and optimization of image sensing toward continuous mobile vision. In *Proceeding of the 11th annual international conference on Mobile systems, applications, and services*, pages 69–82. ACM, 2013.

[15] V. Liu, A. Parks, V. Talla, S. Gollakota, D. Wetherall, and J. R. Smith. Ambient backscatter: Wireless communication out of thin air. SIGCOMM '13.

[16] S. Naderiparizi, M. Hessar, V. Talla, S. Gollakota, and J. R. Smith. Towards battery-free hd video streaming. In *15th USENIX Symposium on Networked Systems Design and Implementation (NSDI 18)*, 2018.

[17] S. Naderiparizi, M. Hessar, V. Talla, S. Gollakota, and J. R. Smith. Towards battery-free hd video streaming. In *15th USENIX Symposium on Networked Systems Design and Implementation (NSDI 18)*, 2018.

[18] S. Naderiparizi, Z. Kapetanovic, and J. R. Smith. Wispcam: An rf-powered smart camera for machine vision applications. In *Proceedings of the 4th International Workshop on Energy Harvesting and Energy-Neutral Sensing Systems*, pages 19–22. ACM, 2016.

[19] S. Naderiparizi, A. N. Parks, Z. Kapetanovic, B. Ransford, and J. R. Smith. Wispcam: A battery-free rfid camera. In *RFID (RFID), 2015 IEEE International Conference on*, pages 166–173. IEEE, 2015.

[20] S. Naderiparizi, P. Zhang, M. Philipose, B. Priyantha, J. Liu, and D. Ganesan. Glimpse: A programmable early-discard camera architecture for continuous mobile vision. In *Proceedings of the 15th Annual International Conference on Mobile Systems, Applications, and Services*, pages 292–305. ACM, 2017.

[21] S. Naderiparizi, Y. Zhao, J. Youngquist, A. P. Sample, and J. R. Smith. Self-localizing battery-free cameras. In *Proceedings of the 2015 ACM International Joint Conference on Pervasive and Ubiquitous Computing*, pages 445–449. ACM, 2015.

[22] S. K. Nayar, D. C. Sims, and M. Fridberg. Towards self-powered cameras. In *Computational Photography (ICCP), 2015 IEEE International Conference on*, pages 1–10. IEEE, 2015.

[23] A. N. Parks, A. Liu, S. Gollakota, and J. R. Smith. Turbocharging ambient backscatter communication. *ACM SIGCOMM Computer Communication Review*, 44(4):619–630, 2015.

[24] A. N. Parks, A. P. Sample, Y. Zhao, and J. R. Smith. A wireless sensing platform utilizing ambient rf energy. In *Power Amplifiers for Wireless and Radio Applications (PAWR), 2013 IEEE Topical Conference on*, pages 160–162. IEEE, 2013.

[25] A. N. Parks and J. R. Smith. Sifting through the airwaves: Efficient and scalable multiband rf harvesting. In *RFID (IEEE RFID), 2014 IEEE International Conference on*, pages 74–81. IEEE, 2014.

[26] M. Rubenstein, A. Cornejo, and R. Nagpal. Programmable self-assembly in a thousand-robot swarm. *Science*, 345(6198):795–799, 2014.

[27] A. Sample and J. R. Smith. Experimental results with two wireless power transfer systems. In *Radio and Wireless Symposium, 2009. RWS'09. IEEE*, pages 16–18. IEEE, 2009.

[28] H. Singh, E. D. D. J, H. S. Rawat, and R. George. *Fundamentals of EM Design of Radar Absorbing Structures (RAS)*. Springer, 2018.

[29] J. R. Smith, A. P. Sample, P. S. Powledge, S. Roy, and A. Mamishev. A wirelessly-powered platform for sensing and computation. In *International Conference on Ubiquitous Computing*, pages 495–506. Springer, 2006.

[30] V. Talla, M. Hessar, B. Kellogg, A. Najafi, J. R. Smith, and S. Gollakota. Lora backscatter: Enabling the vision of ubiquitous connectivity. *Proc. ACM Interact. Mob. Wearable Ubiquitous Technol.*, 2017.

[31] V. Talla, B. Kellogg, S. Gollakota, and J. R. Smith. Battery-free cellphone. *Proceedings of the ACM on Interactive, Mobile, Wearable and Ubiquitous Technologies*, 1(2):25, 2017.

[32] V. Talla, B. Kellogg, B. Ransford, S. Naderiparizi, S. Gollakota, and J. R. Smith. Powering the next billion devices with wi-fi. In *Proceedings of the 11th ACM Conference on Emerging Networking Experiments and Technologies*, page 4. ACM, 2015.

[33] V. Talla and J. R. Smith. Hybrid analog-digital backscatter: A new approach for battery-free sensing. In *RFID (RFID), 2013 IEEE International Conference on*, pages 74–81. IEEE, 2013.

[34] S. J. Thomas and M. S. Reynolds. A 96 mbit/sec, 15.5 pj/bit 16-qam modulator for uhf backscatter communication. In *2012 IEEE International Conference on RFID (RFID)*, pages 185–190. IEEE, 2012.

[35] P. Zhang and D. Ganesan. Enabling bit-by-bit backscatter communication in severe energy harvesting environments. In *NSDI*, pages 345–357, 2014.

[36] P. Zhang, P. Hu, V. Pasikanti, and D. Ganesan. Ekhonet: High speed ultra low-power backscatter for next generation sensors. In *Proceedings of the 20th annual international conference on Mobile computing and networking*, pages 557–568. ACM, 2014.